

## Supporting Information

### **Observation of Nanometer-Sized Electro-Active Defects in Insulating Layers by Fluorescence Microscopy and Electrochemistry.**

Christophe Renault<sup>a,b</sup>, Kyle Marchuk<sup>a,b</sup>, Hyun S. Ahn<sup>b</sup>, Eric J. Titus<sup>b</sup>, Jiyeon Kim<sup>b</sup>, Katherine A. Willets<sup>\*b,c</sup>, Allen J. Bard<sup>\*b</sup>

<sup>a</sup> These authors contributed equally to the present work.

<sup>b</sup> Center for Electrochemistry, Department of Chemistry, The University of Texas at Austin, Austin, Texas 78712, United States

<sup>c</sup> Current address: Department of Chemistry, Temple University, 1901 N. 13<sup>th</sup>. St. Philadelphia, Pennsylvania 19122, United States

## Table of content

Figure S1-----	Passivation of UME with TiO <sub>2</sub> -----	p3
Figure S2-----	Absorbance and emission spectra of CTC -----	p4
Figure S3-----	Cyclic voltametry of CTC -----	p4
Figure S4-----	Chronoamperometry of CTC -----	p5
Figure S5-----	Approach curve -----	p5
Figure S6-----	Photo-bleaching of CTC -----	p6
Figure S7-----	Approach curve -----	p7
Figure S8-----	Fluo. images of UMEs -----	p8
Figure S9-----	Comparison of Fluo. and SEM -----	p9
Figure S10-----	Geometry of the numerical simulation -----	p10
Table S1-----	Parameters of the numerical simulation -----	p11
Movie S1-----	Reduction of CTC on a UME -----	p9

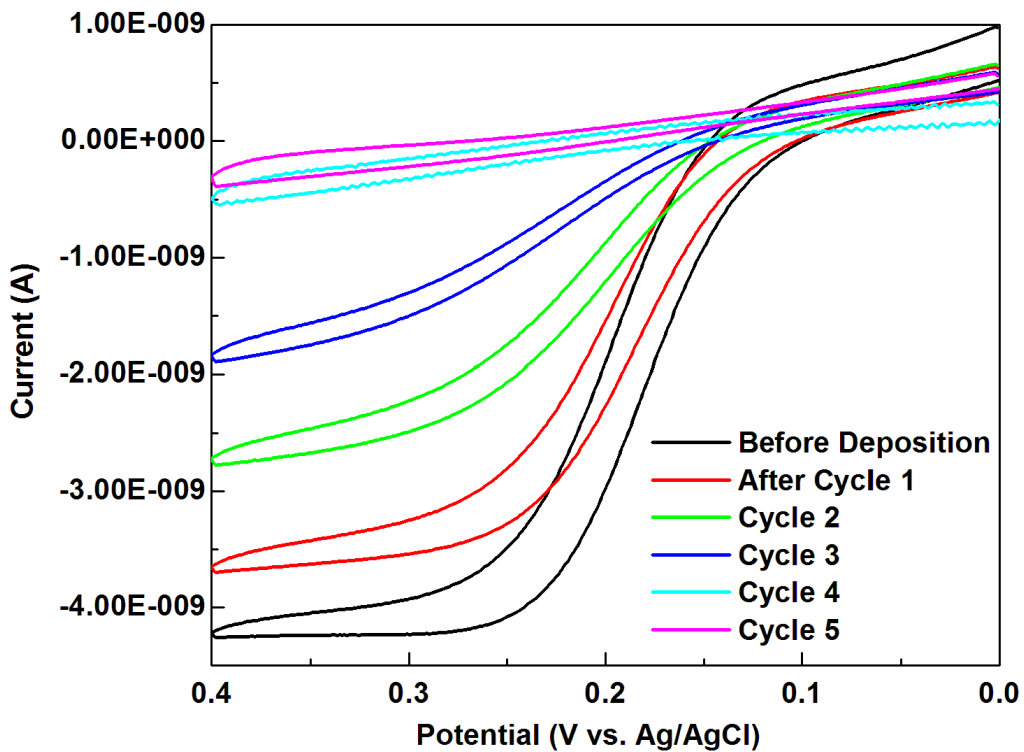


**Figure S1.** Passivation of a 25 μm diameter Pt UME with TiO<sub>2</sub> monitored by cyclic voltammetry. The CVs are recorded at 50 mV/s in a 1.2 mM FcDM in 50 mM pH7 phosphate buffer. The CVs are recorded before and after each cycle of electro-deposition of TiO<sub>2</sub>.

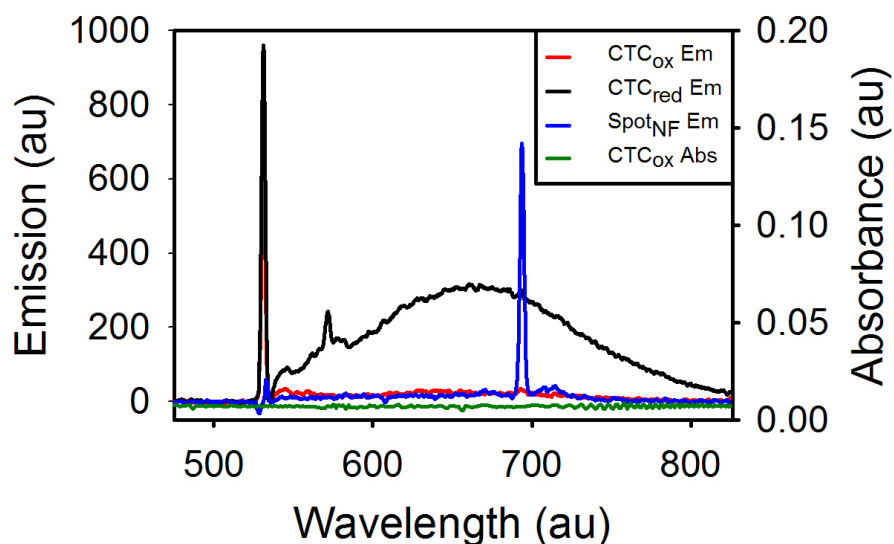


**Figure S2.** Absorbance of  $\text{CTC}_{\text{ox}}$  (green line), fluorescence emission of  $\text{CTC}_{\text{ox}}$  (red line),  $\text{CTC}_{\text{red}}$  (black line), and a non-fluorescent spot (SpotNF, blue line). All emission spectra are background subtracted and taken at the UME. They are the sum of 5 spectra each exposed for 1 second. The large peaks seen at  $\sim 532$  nm is due to laser scatter leaking through the filter set. The absorbance and the emission of  $\text{CTC}_{\text{ox}}$  are both near zero as expected for a non-fluorescent species. After reduction, the emission of  $\text{CTC}_{\text{red}}$  is  $\sim 665$  nm.

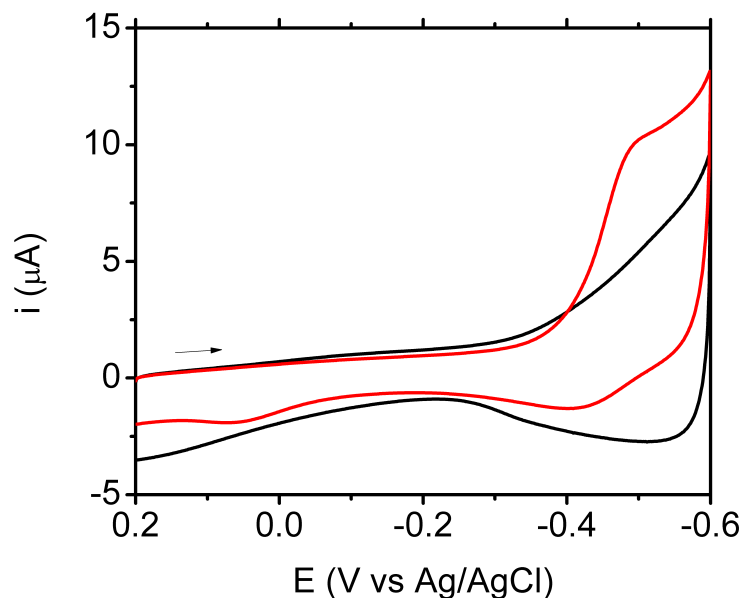


**Figure S3.** Cyclic voltammogram recorded with a 1 mm diameter Pt electrode in absence (black curve) and in presence (red curve) of of 0.5 mM CTC.  $\nu = 50$  mV/s. The experiment is carried out in a 0.1 M pH 7 phosphate buffer degased with Ar.

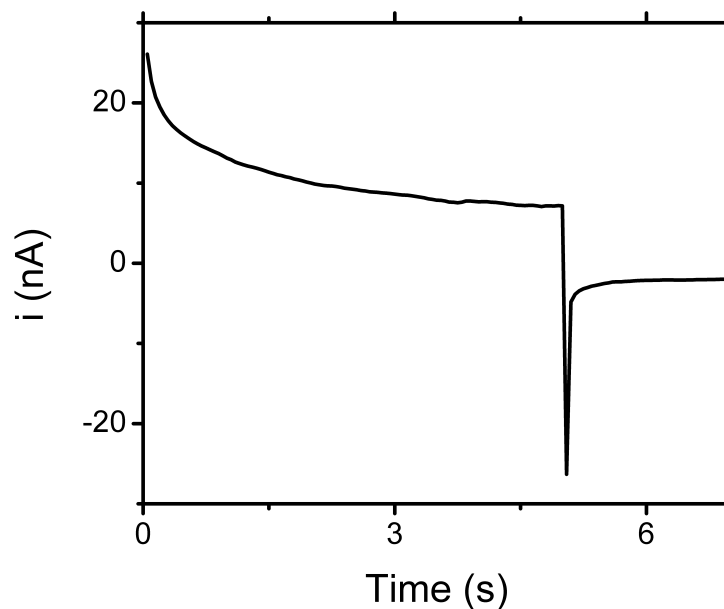


**Figure S4.** Chronoamperogram of a 25  $\mu\text{m}$  diam Pt UME biased 5 s at -0.6 and then 0.2 V for 2 s in a solution of 0.5 mM CTC in 0.1 M pH 7 phosphate buffer.

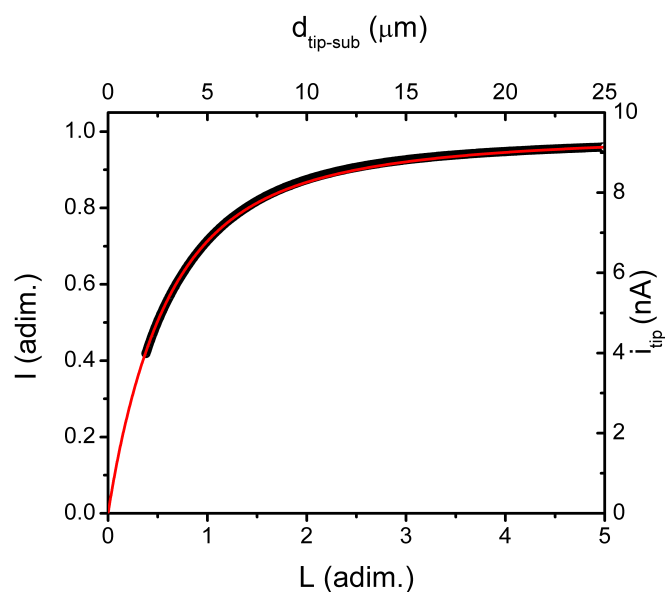


**Figure S5.** Approach curve recorded before taking the image shown in Figure 2d. The approach is realized on the glass sheath and thus a negative feedback is observed. The Au tip is 10  $\mu\text{m}$  in diameter and the concentration of FcDM is 4.7 mM in 0.1 M  $\text{KNO}_3$ . The approach is realized at 200 nm/s. The red curve is a fit of the experimental data (black dots) with a model for negative feedback and a RG of 3.<sup>1</sup>

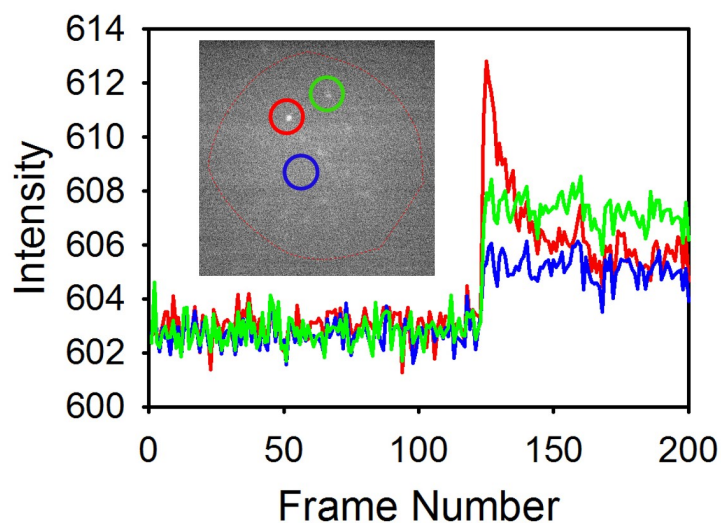


**Figure S6.** Intensity vs frame number for a pinhole defect where CTC has been deposited (red), a background region where no deposition occurred (blue), and a non-fluorescent background spot (green). This intensity time trace represents a typical experimental run. The first ~125 frames represent the time the CTC is being reduced on the electrode without laser illumination. The intensity for all three circled areas increases when laser illumination is introduced at time ~120 s. The pinhole region (red) shows a typical exponential fluorescence intensity decrease associated with photo-bleaching. The background intensity (blue) increases with laser illumination due to leakage of the laser light onto the detector, but stays constant over time. Spots above background like the typical one circled in green are seen on a few of the electrode surfaces. Due to the fact that the spots appear before CTC reduction and have a constant intensity upon laser illumination, we are confident we are not seeing reduced CTC and therefore these sites do not represent pinholes but some other non-electro-active surface feature associated with TiO<sub>2</sub> passivated UMEs.

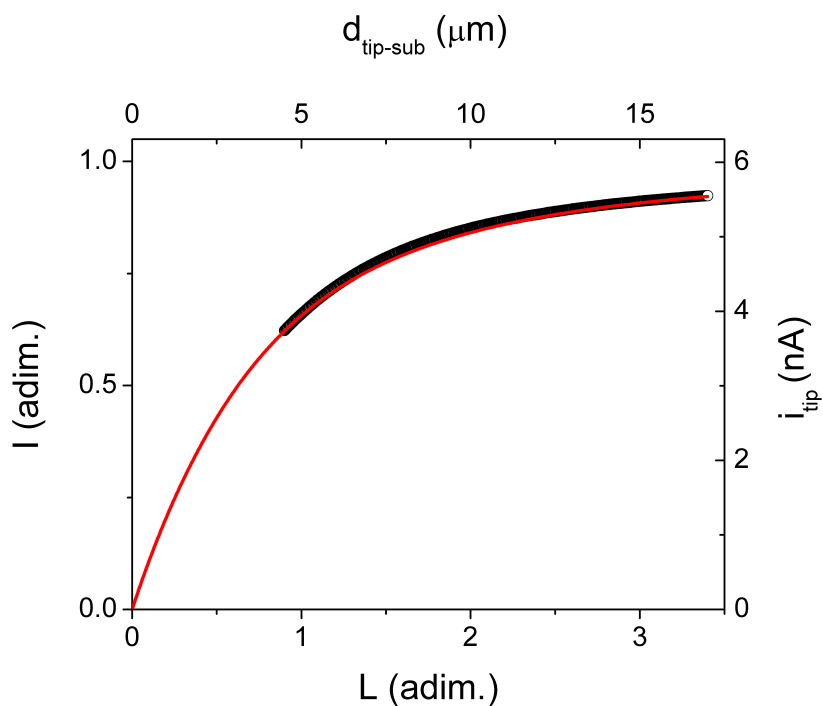


**Figure S7.** Approach curve recorded before taking the image shown in Figure 2h. The approach is realized on the glass sheath and thus a negative feedback is observed. The Au tip is 10  $\mu\text{m}$  in diameter and the concentration of FcDM is 4.7 mM in 0.1 M  $\text{KNO}_3$ . The approach is realized at 200 nm/s. The red curve is a fit of the experimental data (black dots) with a model for negative feedback and a RG of 3.<sup>1</sup>

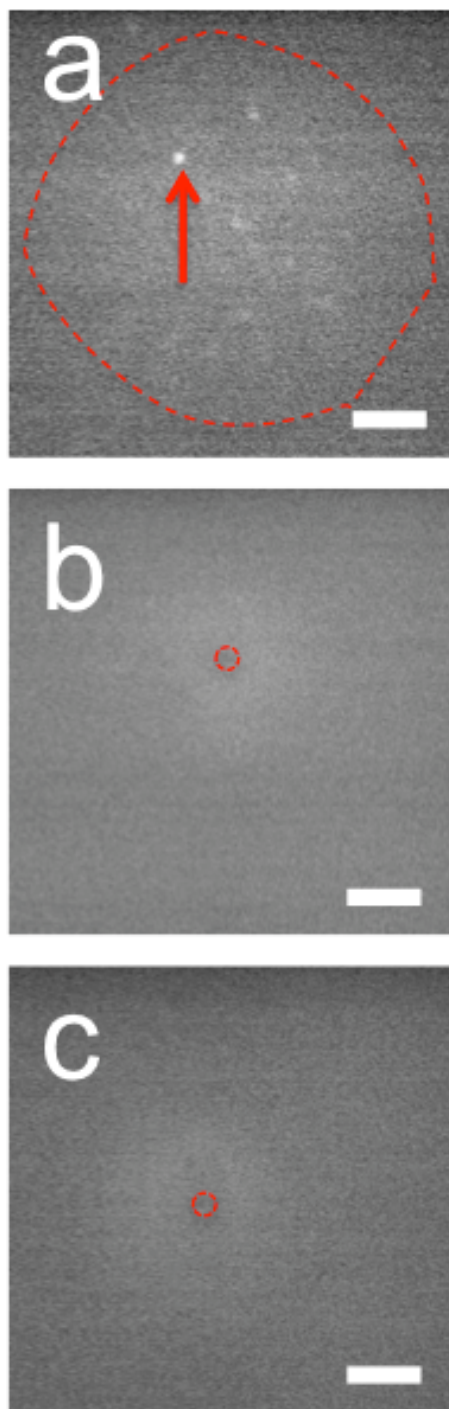


**Figure S8.** Fluorescence micrographs of (a) a passivated 25  $\mu\text{m}$  Pt UME with  $\theta = 99.6\%$  and (b, c) two passivated 1.3  $\mu\text{m}$  Pt UME with  $\theta = 99.8\%$  and  $99.7\%$ , respectively. These micrographs are taken after reduction of CTC. The scale bars represent 5  $\mu\text{m}$  and the red dashed lines indicate the position of the electrode. The arrow in (a) shows the location of the electro-active defect evidenced by fluorescence. In (b) and (c) no fluorescence is detected at the UME surface.



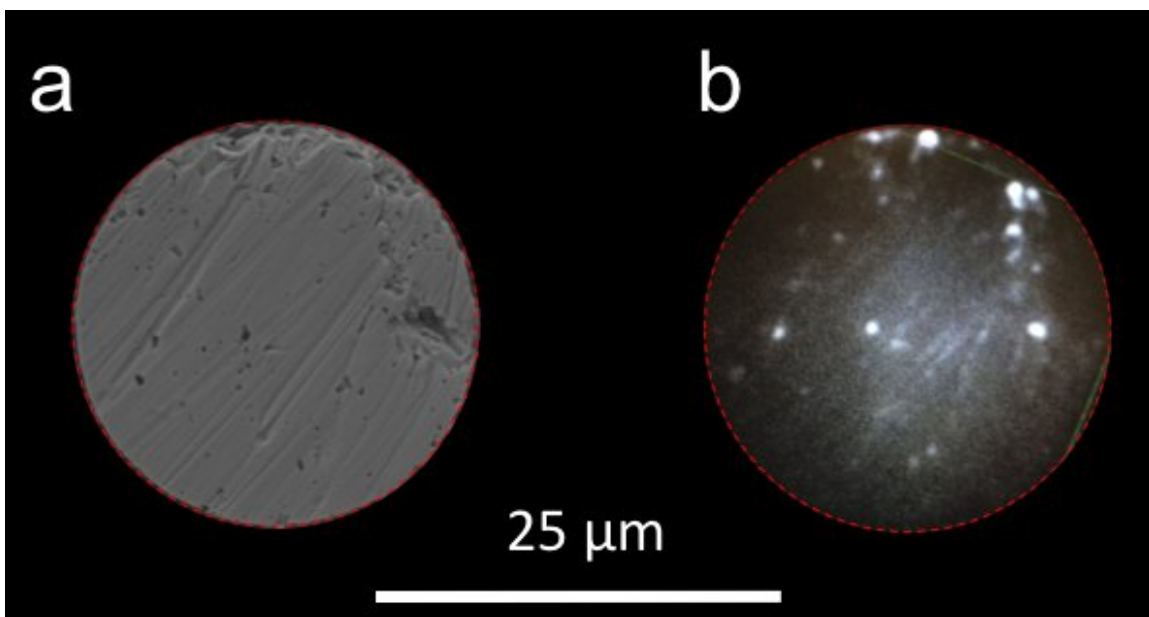


**Figure S9.** (a) SEM image and (b) fluorescence micrograph of a  $\theta \approx 96\%$  passivated 25  $\mu\text{m}$  Pt UME after reduction of CTC. The position of the fluorescent spots in (b) can be correlated with the position of large topographic defects seen in (a).

**Movie S1.** Reduction of CTC over a 25  $\mu\text{m}$  diameter Pt UME. The potential is swept from 0 V to -0.6 V and back to 0 V at 20 mV/s. The movie is played at real speed.

**Numerical simulation.** Numerical simulations were performed using a Dell Precision T7500 Simulation workstation outfitted with Dual Six Core Intel Xeon Processors (2.40 GHz) and 24 GB of RAM. Simulations were carried out using the COMSOL Multiphysics v4.3b commercial package. All simulations were performed in 3D with a time-dependent solver.

The geometry of the problem is represented Figure S11. A 10 x 10 x 8  $\mu\text{m}$  (width x depth x height) cube was created to represent the electrochemical cell. On the base of the cube two 33 nm radius circles spaced by 1  $\mu\text{m}$  from center to center (coordinates: (0;-0.5) and (0;0.5)) represents the two electro-active defects.

The meshing of the cell and the electro-active defects is made with tetrahedrons (element size: extra fine) and triangles (maximum element size: 1.5 nm), respectively. The total number of elements in the mesh is 415570.

The boundaries of the problem are defined as follows. All the walls of the cube except the bottom are defined as concentration boundaries with a constant concentration of FcDM set at 5 mM, the bulk concentration ( $C_{ini}$ ). The concentration of FcDM<sup>+</sup> is set at 0 mM. The bottom of the cube is set as a no flux boundary. Finally, the electrodes are described with a concentration boundary where the concentrations of FcDM and FcDM<sup>+</sup> are imposed at 0 mM and 5 mM, respectively. These boundaries represent a case where the electron transfer is fast with respect to the mass transport and thus this later is the kinetic limiting step.

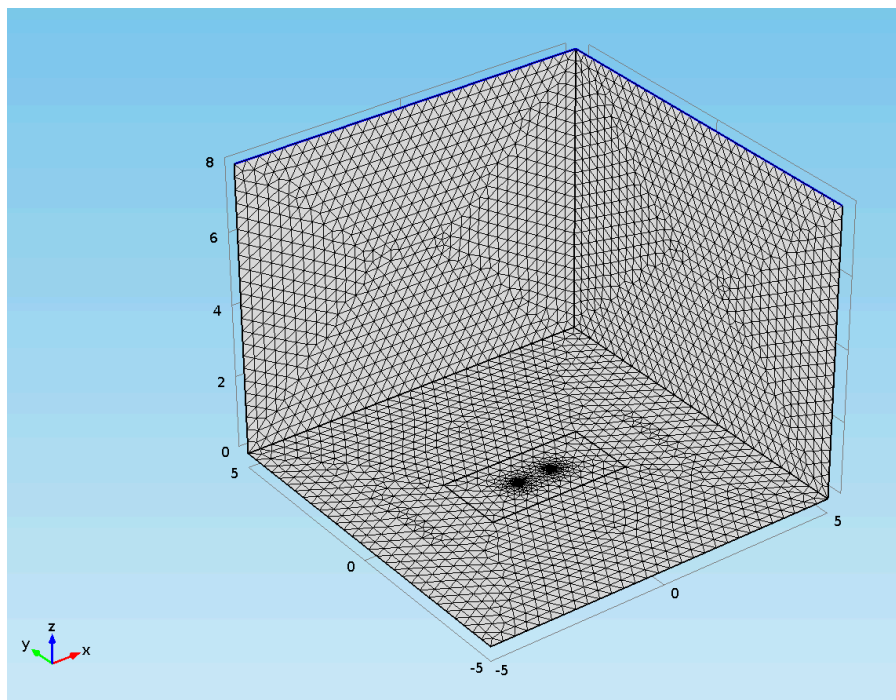


**Figure S10.** Geometry of the cell and the electro-active defects used for the 3D simulation. The distances are in  $\mu\text{m}$ . Three sides of the cells are hidden to show the two electrodes (located where the mesh becomes finer) on the bottom of the cell.

The physic used to describe the mass transport is "Transport of diluted species". The Fick's law is solved for the geometry and boundaries described above and for the two species  $i$ , FcDM and FcDM<sup>+</sup>:

$$\frac{dC_i}{dt} = -\nabla \cdot (-D\nabla C_i)$$

The various parameters of the simulation are gathered in Table S1. The problem is solved with a time-dependent solver at 1 s and 2 s to ensure that a stationary solution is found. The problem was also solved with one of the electrode-active defects having a no-flux boundary condition to suppress its electrochemical response. The current is calculated by integrating the flux of FcDM at the electro-active defect's surface with the equation:

$$i = nFD \iint \frac{dC_{FcDM}}{dz} dx dy$$

For a distance  $L = 1 \mu\text{m}$  between the center of two electro-active defects, the current calculated for one electro-active defect in absence and in presence of a second electro-active defect is 35.3 and 34.6 pA, respectively. The presence of the second electro-active defect decreases by 2% the current obtained for a single electro-active defect. When the defects are separated by  $L = 0.3 \mu\text{m}$ , the current calculated for one electro-active defect in absence and in presence of a second electro-active defect is 35.3 and 33.2 pA, respectively. In that case the presence of the second electro-active defect decreases by 6% the current obtained for a single electro-active defect. The hypothesis of non-interacting electrodes is thus reasonable in both cases.

**Table S1.** Parameters of the 3D simulation.

Parameter	Value	Definition
$n$	1	number of electron
$F$	96485 C/mol	Faraday's constant
$C_{ini}$	5 mM	bulk concentration of FcDM
$D$	$6.7 \times 10^{-6} \text{ cm}^2/\text{s}$	diffusion coefficient of FcDM and FcDM <sup>+</sup>
$L$	0.3 & 1 $\mu\text{m}$	distance between electro-active defects (center to center)
$a$	33 nm	electro-active defects radius
width	10 $\mu\text{m}$	cell's width
depth	10 $\mu\text{m}$	cell's depth
height	8 $\mu\text{m}$	cell's height

---

<sup>1</sup> Bard, A. J.; Mirkin, M. V. *Scanning Electrochemical Microscopy, Second Edition*; second.; CRC Press, 2012.